LINEAR ELECTRIC FIELD CROSS CORRELATION FOR OPTICAL DEVICES

A Thesis

Submitted to the Faculty

of

Purdue University

by

Dan Luu

In Partial Fulfillment of the

Requirements for the Degree

of

Master of Science in Electrical and Computer Engineering

December 2005

TABLE OF CONTENTS

Page

LIST OF FIGURES iii
LIST OF ABBREVIATIONS v
ABSTRACT vi
CHAPTER 1. INTRODUCTION 1
CHAPTER 2. BACKGROUND 3
2.1. Fourier Transform 3
2.2. Cross Correlation Theorem 3
2.3. Auto Correlation (Wiener-Khinchin) Theorem 4
2.4. Truncation 4
2.5. Dispersion 4
2.6. Coherence 5
CHAPTER 3. THEORY 6
3.1. Interference 6
3.2. Auto Correlation 6
3.3. Cross Correlation 7
3.4. Arrayed Waveguide Gratings 8
CHAPTER 4. EXPERIMENT 10
4.1. Experimental Setup 10
4.2. Measurements 14
CHAPTER 5. POLARIMETER 32
LIST OF REFERENCES 33

LIST OF FIGURES

Figure Page

3.1: Representative schematic of Autocorrelation setup 9

3.2: Arrayed waveguide grating diagram [15] 9

4.1: Photograph of auto correlation setup 18

4.2: Output of interferometer vs time with stage set to move at a fixed speed 18

4.3: Number of samples per zero crossing 19

4.4: Measured spectrum without correction by reference 19

4.5: Photograph of cross correlation setup 20

4.6: Measured spectrum with stage at 1 mm/s 20

4.7: Measured spectrum with stage at .5 mm/s 21

4.8: Measured spectrum with stage at .1 mm/s 21

4.9: Output of interferometer with zero nominal stage movement 22

4.10: Output of interferometers with zero nominal stage movement 22

4.11: Group delay with setup alone and with DCF 23

4.12: Interferogram of cross correlator alone 23

4.13: Interferogram of DCF in cross correlator 24

4.14: Dispersion of setup alone and with DCF 24

4.15: Interferogram of flat topped AWG 25

4.16: Detail view of Fig. 4.15: Interferogram of flat topped AWG 25

4.17: Spectrum of AWG vs. OSA measurement of source 26

4.18: Detail view of Fig. 4.17 26

4.19: Spectrum of first and last pulse 27

4.20: Group delay of pulse through each guide 27

4.21: Comparison of normalized group delay 28

4.22: Group delay of peak frequency 28
4.23: Group delay error 29
4.24: Derivative of fitted phase (3d order polynomial) vs. group delay 29
4.25: Linear phase of each guide 30
4.26: ϕ_0 with linear phase term removed 30
4.27: Measured AWG output vs. OSA reference measurement 31
5.1: Polarimeter setup 34
5.2: Depenendcy graph of original setup 34
5.3: Dependency graph of modified setup 35
5.4: Polarimeter measurement at different speeds [11] 35

LIST ABBREVIATIONS GLOSSARY

AWG	Arrayed waveguide grating
DCF	Dispersion compensated fiber
DSF	Dispersion shifted fiber
FFT	Fast Fourier transform
FLC	Ferroelectric liquid crystal
FROG	Frequency resolved optical gating
FSR	Free spectral range
HeNe	Helium neon
OS	Operating system
OSA	Optical spectrum analyzer
PMD	Polarization mode dispersion
RHC	Rght hand circular
SMF	Single mode fiber
SPIDER	Spectral phase interferometry for direct electric field reconstruction
WDM	Wavelength division multiplexing

ABSTRACT

Luu, Dan. M.S.E.C.E. Purdue University, December 2005. Linear Electric Field Cross Correlation for Optical Devices. Major Professor: Andrew M. Weiner.

Accurately measuring phase is an important part of characterizing optical devices. In particular, phase errors are a major cause of non idealities in arrayed waveguide gratings. This thesis presents the design and implementation of an electric field cross correlator, a device which is capable of determining the magnitude and phase response of optical devices.

Measurements of the spectral magnitude and phase of single mode fiber, dispersion compensating fiber, and arrayed waveguide gratings from the cross correlator are presented.

This thesis also includes work on optimization of the control for a compact wavelength parallel polarimeter in order to allow operation at up to 1.25 kHz while measuring 256 wavelengths in parallel. This polarimeter can be used for sensing of polarization mode dispersion, which is a limiting factor in high speed long haul optical fiber telecommunications.

CHAPTER 1. INTRODUCTION

Correlation measurements are used to find the magnitude and phase of optical signals [1][2]. The most conceptually straightforward type of correlation is linear field correlation, which is based on the interference of two beams propogating collinearly. The spectrum and difference in phase between the two beams can be calculated by a Fourier transform, so the technique is also commonly called Fourier transform spectroscopy. Field correlation has many advantages over more complex measurement techniques. Unlike dispersive measurements all frequencies are measured throughout the measurement, which results in a better signal to noise ratio and a faster measurement. Additionally, the resolution is limited only by the movement range of the interferometer. Unlike many intensity correlation techniques, it can uniquely determine the spectral phase, does not require iteration, and does not have problems with convergence. Unlike FROG, no non-linearity is required, so measurements can be done at lower power, and unlike SPIDER, the setup is very simple – it requires just one interferometer [3][4]. The main disadvantage is that a reference is required, and the main difficulty in implementation is that precise mechanical resolution is required [1][5][6].

Since a reference is required, the simplest measurements to take are of devices that pass light so that the input beam can be split and used as a reference. The purpose of this thesis is to build a cross correlator suitable for phase measurements on arrayed waveguide gratings, as well as other optical devices. Previous work in the group includes the construction of the devices to measured, AWGs that generate a pulse train. Intensity correlation as well as power spectrum measurements indicated non idealities, but the extent of phase errors in the devices were unknown [7]. Other previous work in the research group includes the construction of a field autocorrelator, on which the autocorrelator in this thesis is based; the cross correlator in this thesis is based on that

autocorrelator [8]. The construction of a field cross correlator allows optimization of new arrayed waveguide gratings [9][10].

The second chapter covers some preliminary mathematical background. The third chapter details auto correlation and cross correlation and gives some background on arrayed waveguide gratings. The fourth chapter describes the experimental setup and the measurements taken by that setup.

Additionally, there is a fifth chapter which describes the optimization of the control of a high speed wavelength-parallel polarimeter to run at speeds in excess of 1.25 kHz [11].

CHAPTER 2. BACKGROUND

2.1. Fourier Transform

The Fourier transform, $\mathcal{F}$, and its inverse, $\mathcal{F}^{-1}$,can be defined as

$$\mathcal{F}\{h(t)\} = H(f) = \int h(t)e^{-j2\pi ft}df \tag{2.1}$$

$$\mathcal{F}^{-1}\{H(f)\} = h(t) = \int H(f)e^{j2\pi ft}dt. \tag{2.2}$$

2.2. Cross Correlation Theorem

The cross correlation between two functions h(x) and g(x) is

$$f(v) = h(v) \otimes g(v) = \int h^*(u-v)g(u)du = \int h^*(u)g(u+v)du. \tag{2.3}$$

By the correlation theorem,

$$\mathcal{F}\{h^*(x)g(x)\} = H(v) \otimes G(v) = \int H^*(u)G(u+v)du \tag{2.4}$$

$$\mathcal{F}^{-1}\{H^*(v)G(v)\} = h(x) \otimes g(x) = \int h^*(u)g(u+v)du. \tag{2.5}$$

i.e., the Fourier transform of the conjugate of a function multiplied by another function is the cross correlation of the two functions. This is similar to the convolution theorem, which states that the Fourier transform of the product of two functions is the convolution of the two functions [12].

2.3. Auto Correlation (Wiener-Khinchin) Theorem

In the special case that h and g are the same function the cross correlation theorem reduces tot he auto correlation theorem. Letting $h = g$, the result is:

$$\mathcal{F}^{-1}\{|H^2(\nu)|\} = h(t) \otimes h(t) \tag{2.6}$$

In other words $|H^2(\nu)|$, the Fourier transform of the power spectrum, is the autocorrelation of the function with itself [12].

2.4. Truncation

Truncation of a signal can be represented as multiplication by the rectangle function, scaled to an appropriate length. The rectangle function can be defined as

$$\Pi(x) = \begin{cases} 0, |x| > X \\ .5, |x| = X \\ 1, |x| < X \end{cases} \tag{2.7}$$

Multiplication in the time-domain is equivalent to convolution in the frequency domain. Since the Fourier transform of the rectangle function is the sinc function the resultant spectrum is the sinc function convolved with the original untruncated spectrum, $H_t(\nu) = 2X\text{sinc}(2\pi\nu)H(\nu)$ [12].

2.5. Dispersion

According to the Fourier shift theorem, multiplying a signal by $e^{-j\omega\tau}$ in the frequency domain is equivalent to delaying that signal by τ in the time domain. In general, τ can be arbitrary and the group delay, $\tau(\omega)$, can be defined as

$$\tau(\omega) = -\frac{\partial\phi(\omega)}{\partial\omega}. \tag{2.8}$$

If the signal is a pulse and different frequencies have different delays the pulse will become dispersed, so the dispersion is defined as

$$D(\omega) = -\frac{\partial^2 \phi(\omega)}{\partial \omega^2}. \tag{2.9}$$

The phase can be Taylor expanded about some frequency ω_0 and written as

$$\phi(\omega) = \phi_0 + \phi_1(\omega - \omega_0) + \frac{\phi_2}{2!}(\omega - \omega_0)^2 + ..., \tag{2.10}$$

where $\phi_i = \left.\frac{\partial^i \phi(\omega)}{i! \partial \omega^i}\right|_{\omega_0}$ is called the ith order phase [1].

2.6. Coherence

Coherence refers to the degree that a field has a fixed phase relationship. For a pulse with some bandwidth, δ_ν, the coherence time is approximately $\tau_c = 1/\delta_\nu$. If a beam is split and then recombined, the resulting field can be calculated as the sum of the fields and intereference is said to occur if the difference in propagation time between the light in the two paths is less than the coherence time. Otherwise, the phase relationship between the two paths will effectively be random and the resulting intensity can be calculated as the sum of the intensities. For light moving at some speed c, the coherence length can be defined as $l_c = \tau_c c = c/\delta_\nu$. Interference will occur if the path length difference is less than the coherence length [13].

CHAPTER 3. THEORY

3.1. Interference

A single frequency wave can be written as

$$E = \mathrm{Re}[C_1 e^{j(kx-\omega t)}], \tag{3.1}$$

where C_1 is the magnitude. The frequency of signals in the optical communications range is between 170 THz and 200 THz, which is too fast for any detector to measure. Since we can't measure E(t) directly, we measure the time average power instead.

Consider two waves, $E_1 = \mathrm{Re}[C_1 e^{j(kx-\omega t)}]$ and $E_2 = \mathrm{Re}[C_2 e^{j(kx-\omega t)}]$, traveling collinearly, with intensities $I_1 = \mid E_1 \mid^2$ and $I_2 = \mid E_2 \mid^2$. Their combined intensity is

$$I_t = I_1 + I_2 + 2\sqrt{I_1 I_2}\cos\phi, \tag{3.2}$$

where ϕ is the difference in phase between the two waves. If $I_1 = I_2$, the result simplifies to

$$I_t = 2I_1(1+\cos\phi)\ [12][1]. \tag{3.3}$$

3.2. Auto Correlation

A Michelson interferometer splits incoming radiation into multiple beams and then recombines the radiation, potentially inducing a path length difference between the beams. A schematic of this is shown in Fig. 3.1. The incoming beam is split at the beam splitter, B, with half being reflected towards M2 and half passing through B, heading towards M1. After they reflect off M1 and M2, the beams come back to B, and half of each beam goes back towards the input, while the other half goes to the output. In

principle, a detector could be placed at the input to capture the light going back in that direction, but this device only uses the light that goes to the output. At the output, the path length difference between the two beams is 2(M1' – M2) $=\delta$. For any given frequency, a path length difference of δ translates into a phase difference of $\phi = 2\pi\delta/\lambda = 2\pi\nu\delta/c$, resulting in an intensity of

$$O = 2I_2(1+\cos(2\pi\nu\delta/c)) \tag{3.4}$$

at the detector, where I_2 is the magnitude of the intensity at that frequency. Ignoring the constant term, the result is

$$O = 2I_2\cos(2\pi\nu\delta/c), \tag{3.5}$$

a sinusoid with minima and maxima every half-wavelength apart.

For non-monochromatic sources all frequencies interfere if the path length difference is less than the coherence length. Given a signal with some spectrum, S(v), the signal at the detector, or the interferogram, will be

$$I(x) = \int S(\nu)\cos(2\pi\nu\delta/c)d\nu, \tag{3.6}$$

where $\delta = 2x$. Because we're only concerned with the real part, $\cos(2\pi\nu\delta/c)$ can be rewritten as $e^{j2\pi\nu\delta}$, which gives

$$I(x) = \int S(\nu)e^{j2\pi\nu\delta}d\nu = \mathcal{F}^{-1}\{S(\nu)\}. \tag{3.7}$$

This says that the Fourier transform of the interferogram is the power spectrum. This also comes out of equation (2.5), the autocorrelation theorem, if $h(x)$ is defined as the electric field of the source. Since taking an autocorrelation measurement is exactly equivalent to measuring the power spectrum i.e. no phase information can be obtained [12][1].

3.3. Cross Correlation

In general, both arms of the interferometer can have different characteristics. This can be represented by considering an interferometer with a device with some transfer function $H(\nu)$ inserted in one arm. Applying the cross correlation theorem and letting

the path through the device arm be h, and the path through the other arm be g, the result is:

$$\mathcal{F}^{-1}\{H^*(\nu)S^*(\nu)S(\nu)\} = h(x) \otimes g(x) = \int h^*(u)g(u+\nu)du\,. \tag{3.8}$$

In other words, the Fourier transform of the interferogram gives $H^*(\nu)|S(\nu)|^2$. As a result, even if both arms of the interferometer are not identical, the transfer function for a device can be obtained by taking a measurement with the device and obtaining $H^*(\nu)|S(\nu)|^2$, and then dividing by $H_r^*(\nu)|S(\nu)|^2$, the result of a measurement without the device, to get $H_d^*(\nu)$ [1].

3.4. Arrayed Waveguide Gratings

AWGs have an input that goes into a slab waveguide which spreads the input beam spatially. The spread out beam is then coupled into a set of waveguides, each of which has a different length, and then into another slab waveguide. The light is again spread out spatially, so some part of the beam from each waveguide can goes into each output. The devices examined in this guide have a differential delay per guide greater than the input pulse width for the sources used, so the AWG acts as a series of delay elements, resulting in a pulse train at the output for a single input pulse, as shown in Fig. 3.2. In contrast, conventional AWGs are created so that the differential delay per guide is shorter than the input pulse width. In this case, the light through each guide arrives at the end of the dispersive array at nearly the same time but with different phase. Different frequencies have different relative phases, so they will constructively interfere at different points in space, and the outputs at the other end of the slab waveguide can be arranged so that each output captures a different frequency range [14][15].

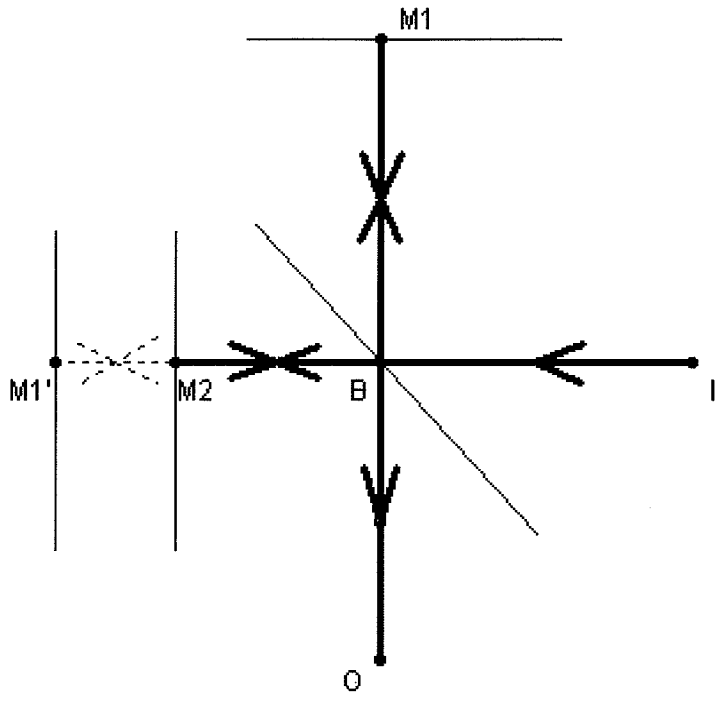

Fig. 3.1: Representative schematic of Autocorrelation setup

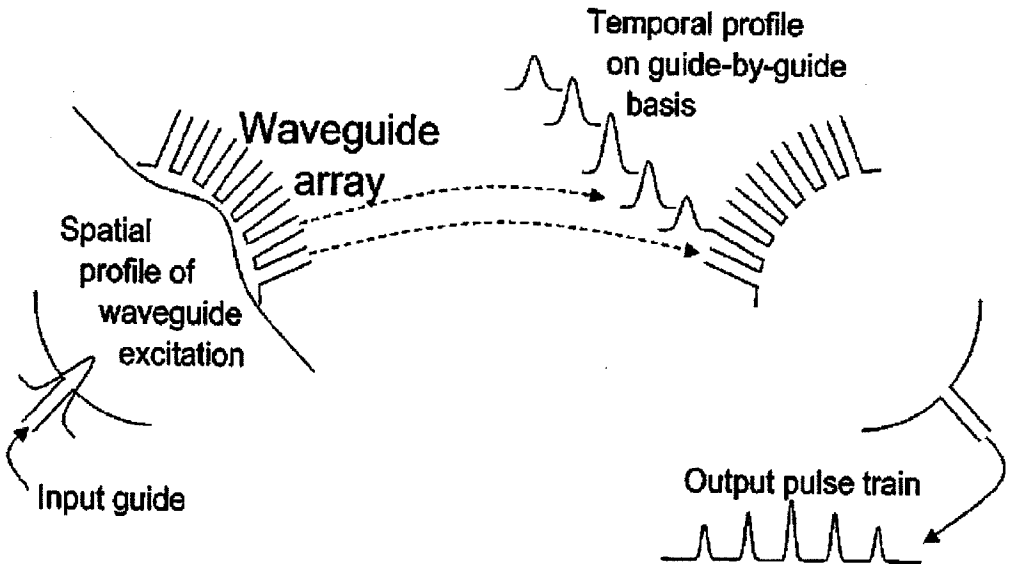

Fig. 3.2: Arrayed waveguide grating diagram [15]

CHAPTER 4. EXPERIMENT

4.1. Experimental Setup

The autocorrelator was built with two adjacent interferometers which share the same control for the movement of the mirrors. In terms of the simplified schematic shown in Fig. 3.1, M1 is replaced by a corner cube retroreflector, and M2 is replaced by a set of mirrors which displace the beam laterally exactly as much as the retroreflector does. The retroreflector reduces the effect of misalignment by ensuring that the incoming and reflected beams are parallel to each other. The motion of the retroreflector is controlled by a (Newport UTM 150 CC.1) one-dimensional movement stage using a DC servo motor; the stage has a range of 15 cm. The signal side uses a 2" diameter non polarizing beam splitter, and the reference side uses a 2" diameter beam splitter of unknown type. On the signal side, the beam comes from a fiber input which goes into a collimator; the rest of the setup is in free space, and after passing through the interferometer the beam goes into a (Thorlabs DET 410) high speed InGaAs photodetector. There is space for a polarizer just after the collimator on the signal side in case the source being used for a particular experiment is unpolarized. On the reference side, the beam comes from a 632.8nm HeNe laser, and the output is a (Thorlabs DET 110) high speed silicon photodetector. The setup is covered by a box to reduce the effect of air movement and stray light. Both photodetectors are connected to an analog-to-digital card in the computer that records the data. The photodetectors sample at a fixed frequency which nominally corresponds to one for every 5nm of retroreflector movement; in practice there is variation in the speed of movement of the retroreflectors. A photograph of the setup is shown in Fig. 4.1. Software was created to control the movement of the stage, sample the photodetectors at the correct rate, record the data, and

display the resulting interferograms in real time. The software talks to a GPIB card which controls the movement stage via a (Newport ESP 300) motion controller, and an (National Instruments 6111) analog to digital converter card which samples the photodetectors.

The autocorrelator requires the second interferometer, which is used as a reference, because the speed of the stage can vary by as much as a factor of five during normal operation. Fig. 4.2 shows a plot of the reference when the stage is set to a constant speed and the sampling rate of the photodetector is fixed. Since the reference used is (approximately) monochromatic, the signal obeys the relationship in equation (3.4). Ideally, the plot would be a perfect sinusoid. Instead, the plot shows a sinusoid which is compressed and stretched over some regions, indicating a speed variation over the range. Fig. 4.3 shows the number samples between zeros of the reference over a typical scan, which is directly proportional to the time required to move the 316.4 nm between each zero. The variance in speed decreases as the speed of the stage increases, but not enough to give a precise measurement without correcting for the changes in speed.

If a spectrum is calculated without correcting for the changes in the speed of the stage i.e. if it is assumed the samples are equally spaced in distance, the resulting spectrum shows little resemblance to the real spectrum (though its peak is, on average, centered around the peak of the real spectrum). Fig. 4.4 shows such a spectrum, as well as a reference spectrum taken by an OSA. All of the reference graphs shown in this thesis were taken by the same OSA, an Ando AQ6317B.

Initially, the following algorithm was used to calculate position: normalize the reference so that the range is from -1 to 1 over each half period from each extremum to the next, find all of the zero crossings, and then use the arcsine of the value as well as the number of zeros crossed to find the exact position of each sample. This normalization was required due to slow (10+ s period) but large (25%) power variations in the reference laser. Once the position of each sample was known, interpolation with spacing equal to the nominal stage movement speed divided by the sampling rate was done in order to get a set of samples with uniform spacing in distance to do an FFT. This method is effective for autocorrelation measurements of broadband sources. However, the 2 GB memory

limit imposed by MATLAB on Windows systems can pose a problem when using this method on longer interferograms when the interferograms are extended to obtain a suitable resolution in the frequency domain. Sampling an average of once every 10 nm, a 10 cm interferogram has 20 MSamples (80 MB); extending the interferogram to 100 cm to obtain better resolution, the result is an 800 MB interferogram, which doesn't leave space to do the FFT and store the spectrum. For longer interferograms, only one point of data was used per zero crossing (every 316.4nm), interpolating to find the value of the IR signal at the zero of the reference. Since none of the sources used have energy above 210 THz (or below 1428 nm), the sampling could be done more sparsely while meeting the Nyquist criteria. The reduced memory usage does come at a cost: a reduced signal-to-noise ratio [16].

It is also possible to do a Lomb transform directly on the unevenly spaced data, which gives a better signal/noise ratio, but doing that would be slower than interpolating to get evenly spaced data and then computing the FFT [17][18].

The fiber based cross correlator was built by using the reference side of the autocorrelator and removing everything but the retroreflector on the signal side, replacing it with a fiber based setup, as shown in Fig. 4.5. The fiber input goes into a (Newport F-CPL-F 12155 1550) 50/50 fiber coupler instead of a 50/50 beam splitter. One arm of the coupler runs through a (General Photonics Polarite) polarization controller and the device to be tested before going into the second 50/50 coupler. The other arm of the first coupler goes to a collimator which is directed at the retroreflector, and then back into another collimator before going into the second 50/50 coupler. The output of the second coupler runs into a bare fiber adapter which is outputs directly onto a photodetector. Going out of the collimator, off of the retroreflector, and then into the second collimator results in an average of 1dB loss, degrading the fringe contrast slightly. The loss is dependant on both frequency and the position of the stage.

In principle, cross correlation measurements could also have been taken with the autocorrelator setup by inserting a free space device in one of the arms of the autocorrelator.

Time dependent variations can have a greater effect on measurements taken on cross correlation measurements than on auto correlation measurements since dispersion results in a longer interferogram. One potential source of such problems is polarization fluctuation, but measurements taken by an OSA with a polarizer show that there is no noticeable change in polarization vs. frequency over time. Another potential source of problems are path length changes, potentially caused by vibration, air currents, or other factors. A measurement taken while the interferometer is fixed is shown in Fig. 4.9. Ideally, there would be no optical path length change over time when the stage is fixed, and the plots would show a constant input. The device side shows 100% variation in 5-10s, while the reference side shows 30% variation in 10-20s. As shown in Fig. 4.10, both devices also have variations on a shorter time scale. On the device side, there is a fast 10% variation, and on the reference there is a fast 30% variation. The oscillations on the device (IR) side are slower than the oscillations on the reference (HeNe) side, but not by the factor of 2.4 that would be expected if the oscillations were caused by an identical optical path length change. One of the IR sources used in the measurements shown sometimes has oscillations of up to 2%, but that can't account for the oscillations seen. The HeNe laser sometimes has power oscillations of up to 30%, but the oscillations were slower and more predictable than the oscillations seen here.

Moving the stage at a higher speed reduces the effect of the errors caused by these oscillations. Increasing the speed up to .5 mm/s reduces the total error, but beyond that speed the measurement error increases, possibly due to vibrations or instability caused by moving the stage at a speed close to its designed limit. Fig. 4.6, Fig. 4.7, and Fig. 4.8 show the resultant calculated spectral magnitude when measurements are taken with the stage at nominal speeds of 1mm/s, .5 mm/s, and .1 mm/s. There is a substantial phase error where the measured power spectrum is near zero, but otherwise the phase error is relatively insensitive to the stage speed.

In the cross correlation setup, there is a free space region in the reference arm. Since the total path length through both arms must be the same, there needs to be between 26 cm and 41 cm more fiber in the device arm than the reference arm. A measurement taken with no device in the setup yields the spectrum and phase. The group

delay is found by taking the derivative of the phase, which magnifies the noise in the measurement. Savitzky-Golay smoothing was used when calculating the derivative of the phase [19][20]. The spectrum measured by the correlator is identical to the spectrum shown in Fig. 4.7; the group delay is shown in Fig. 4.11. The dispersion seen from 1.85 THz to 1.95 THz (an 84nm range) is .4 ps. In the case shown here, there was a 29 cm difference in fiber length between the two arms, giving a dispersion figure of 16.4 ps / (nm-km), which is in good agreement with the nominal dispersion figure for SMF of 17 ps / (nm km).

The effect of noise in the measurement could be reduced by using a stage that is stable at higher speeds. Using WDM couplers and an IR source with a frequency outside of the frequency range to be measured, the distance reference could pass through the exact same space as the beam on the signal side. That would eliminate errors from difference between the reference side and the signal side but that would only work with devices where a suitable reference wavelength can be passed through the device.

4.2. Measurements

Cross correlation measurements were taken on various lengths of DCF. The figures shown below are for an unknown length of DCF that is approximately 65 cm. Fig. 4.11 shows the delay of the setup itself, the setup with DCF, and the difference between those two measurements. Since the path length difference between both arms of the interferometer must be maintained, the delay shown is actually the delay of 65 cm of added DCF minus the delay of 65 cm of SMF that was replaced by the DCF. The nominal value of dispersion in SMF is 17 ps/(nm km), and the nominal value for dispersion in the DCF used is 125.8 ps/(nm km), so the nominal change in dispersion is 142.8 ps/(nm km). The measurement shows 8.0 ps of dispersion over a 10 THz range from 185 THz to 195 THz, an 84 nm range, or 146.5 ps/(nm km). The difference between the nominal value and the measured value is less than the uncertainty of the length of the DCF. The dispersion can also be seen in the interferograms, which are shown in Fig. 4.12 and Fig.

4.13. All of the interferograms shown were taken with a nominal sampling rate of 5 nm per sample, or 10 nm of optical path length difference per sample.

The frequency dependant dispersion can be found by taking the derivative of the group delay, but noise dominates that measurement in the current setup. If a cubic polynomial is fitted to the phase, and two derivatives are taken to find a dispersion term, the dispersion slope has the incorrect sign 20% of the time. Precise frequency dependant dispersion can be calculated by averaging multiple measurements. Fig. 4.14 shows a plot of the measured dispersion and the fitted dispersion without averaging.

Cross correlation measurements were also done on three arrayed waveguide gratings. Between the input and output of the device used there is 6.5 m of DSF with unknown parameters and the AWG itself, which is 2.8 cm long. The plots shown are for a device that was designed to produce a square pulse train from a single input pulse. That device has an FSR of 500 GHz (or 2 ps delay per guide) [15].

To match the dispersion, 77.6 cm of DCF was used in the free space arm along with the 523.6 cm of SMF that was required to match the length of the devices. The interferogram for one of the measurements is shown in Fig. 4.15, with detail shown in Fig. 4.16.

Intensity correlation measurements showed that there was some variation in the pulse heights. Since each pulse is cleanly separated in the interferogram, the same variation can be seen in the interferogram and it is consistent with the intensity correlation measurements. Moreover, each pulse can be analyzed separately and the transfer function for the pulse through each guide can be found. The pulses were separated by creating rectangular windows with borders at the minima between pulses. Since there is virtually no overlap between the pulses, the analysis on each pulse can be done as if it is a separate interferogram after zeroing the interferogram outside of the window. The reason the plots shown are for this particular device is that the delay per guide was large enough that it was possible to easily separate each pulse; the other two devices measured had 1 ps delay per guide, so it wasn't possible to dispersion compensate the setup enough to cleanly separate the pulses with the SMF and DCF that

was available. It is possible to extract phase information for each pulse even when the pulses are not cleanly separated, but additional data processing is required. [21].

The spectrum measured by the correlator is shown is shown in Fig. 4.17, with detail shown in Fig. 4.18. Since the pulse train is not perfectly rectangular, each passband is not a perfect sinc function. The measured spectrum of two of the pulses passing through individual guides is shown in Fig. 4.19. As expected, the signal-to-noise ratio of the spectrum from each individual pulse is worse than the signal-to-noise ratio of all of the pulses. Fig. 4.20 shows a plot of the group delay of each pulse. A plot of the group delay through two different guides, adjusted so that the group delays overlap, is shown in Fig. 4.21. After adjusting for the average delay difference per guide, the difference in delay of any particular frequency between guides is at most 29 fs. The difference tends to be greater where the spectrum is weaker, which is consistent with the possibility that the differences are caused by noise in the measurement. Fig. 4.22 shows a plot of the group delay of the peak frequency (1.895 THz) of each guide. There is an average of 2.00 ps delay between each guide. Fig. 4.23 is a plot with the linear term removed, which allows delay errors to be easily seen. The delays of all of the guides are within 2.3 fs of the ideal delays.

Since the parameters of the DSF are unknown, it isn't possible to distinguish between the effects of the AWG and the effects of the DSF, but a large cubic phase term centered on the zero dispersion wavelength of the DSF is expected for DSF alone when compared to the DCF-SMF link that was used to compensate the dispersion. Fitting a cubic polynomial to the phase and then finding the group delay from that fitted phase gives a reasonable fit. Fig. 4.24 shows the group delay from the fitted phase vs. the group delay calculated from the raw phase.

The above plots show non-idealities in 2nd order phase and above, but not in linear phase. Taking the Taylor expansion of the phase as in equation (2.10), a term that is linear in guide number is expected. The linear phase of each guide is shown in Fig. 4.25 and the error, which is found by subtracting the linear relationship between guides, is shown in Fig. 4.26.

As a check on the accuracy of phase measurement, the transfer function measured by the cross correlator was checked against the spectrum measured by an OSA. A plot of the results is shown in Fig. 4.27. Since the relative intensities of each pulse match the results of the intensity correlation measurements, the accuracy of the spectrum is a good indication of the accuracy of the phase.

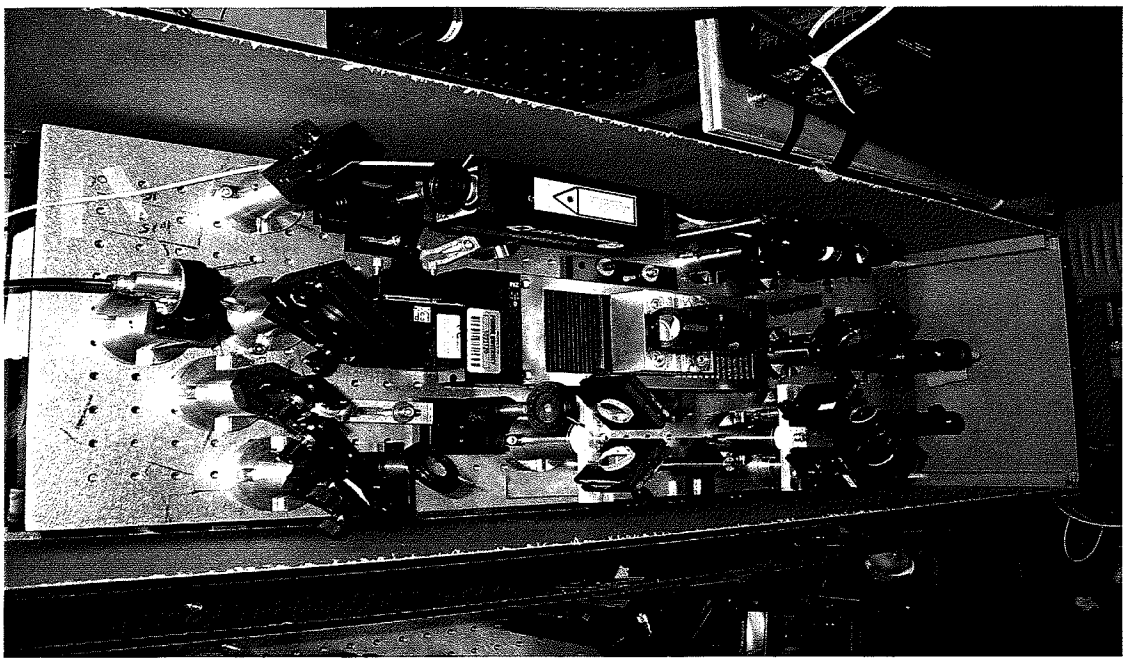

Fig. 4.1: Photograph of auto correlation setup

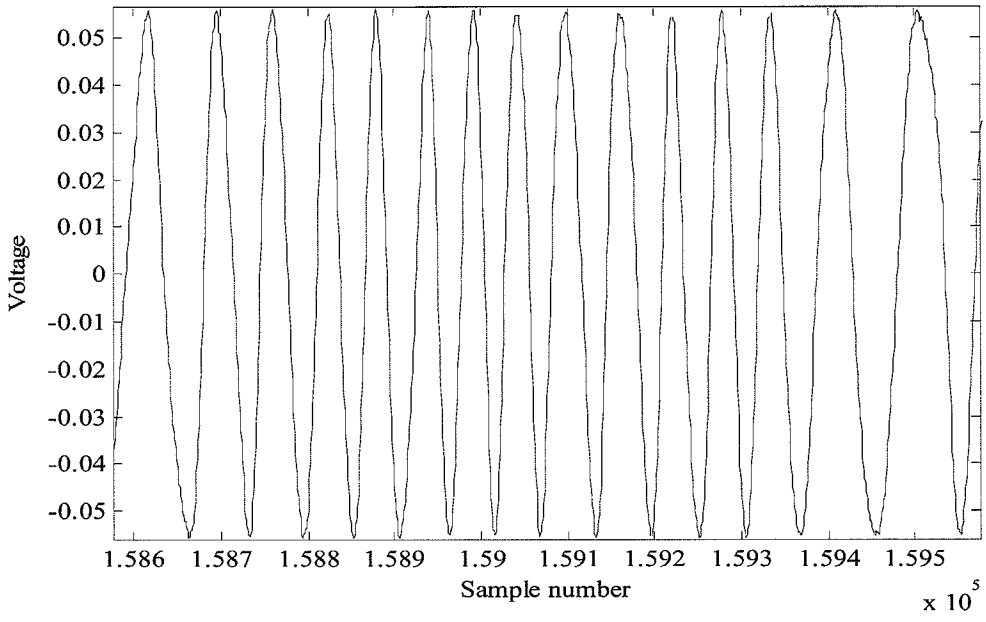

Fig. 4.2: Output of interferometer vs. time with stage set to move at a fixed speed

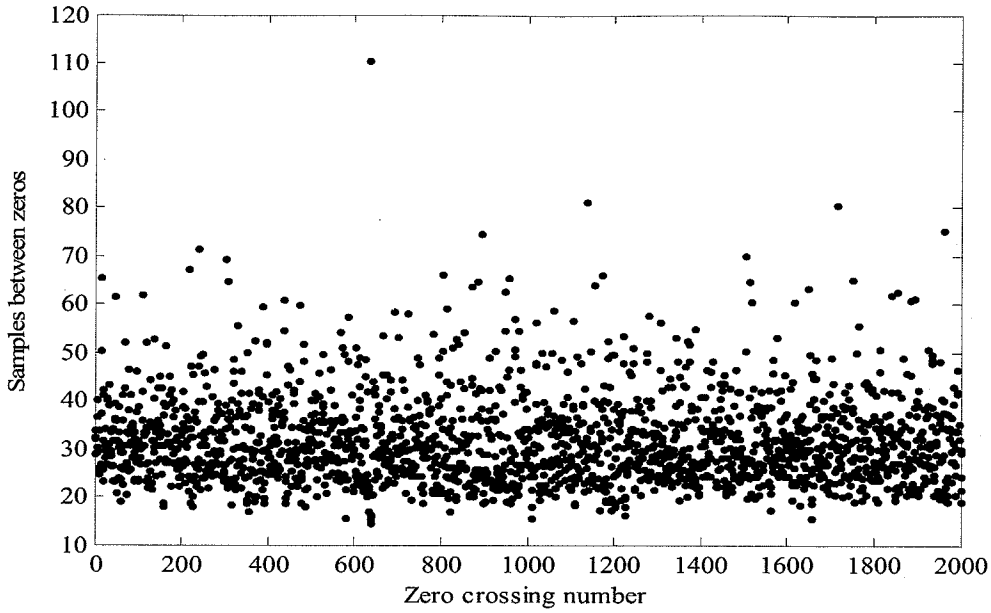

Fig. 4.3: Number of samples per zero crossing

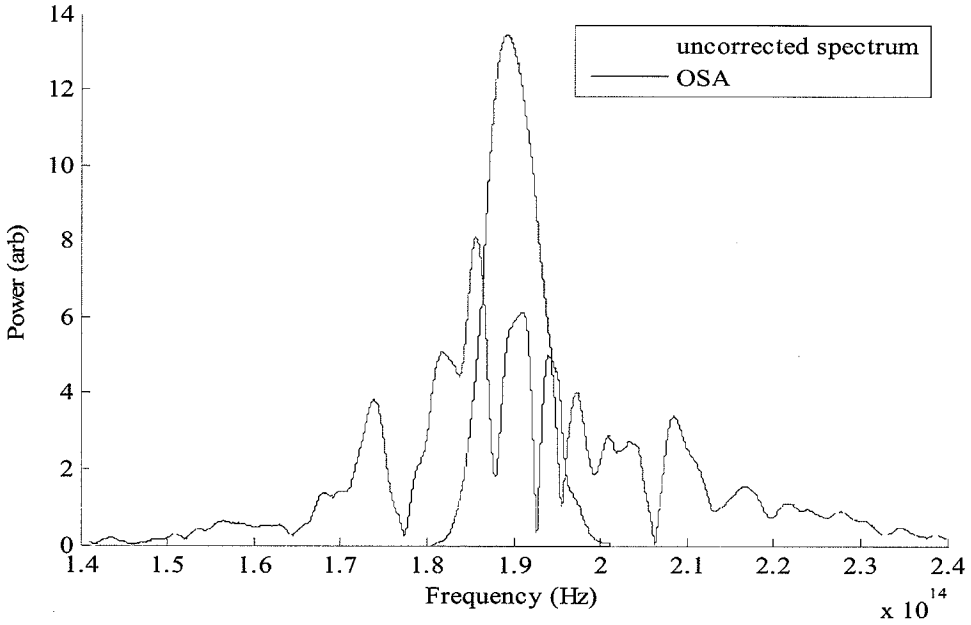

Fig. 4.4: Measured spectrum without correction by reference

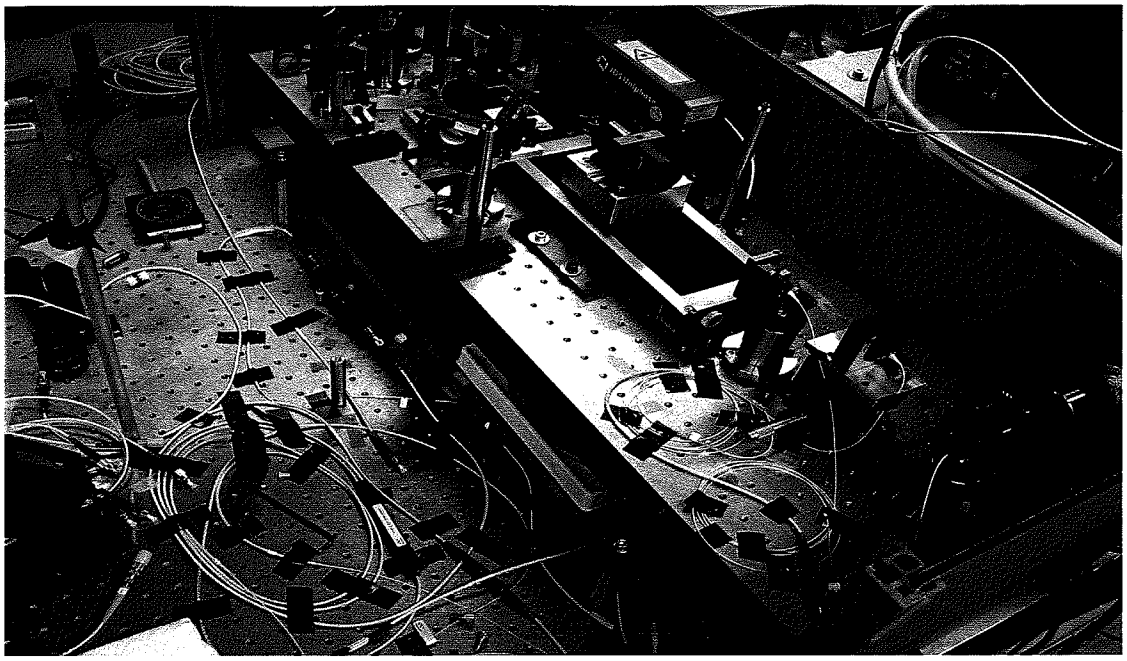

Fig. 4.5: Photograph of cross correlation setup

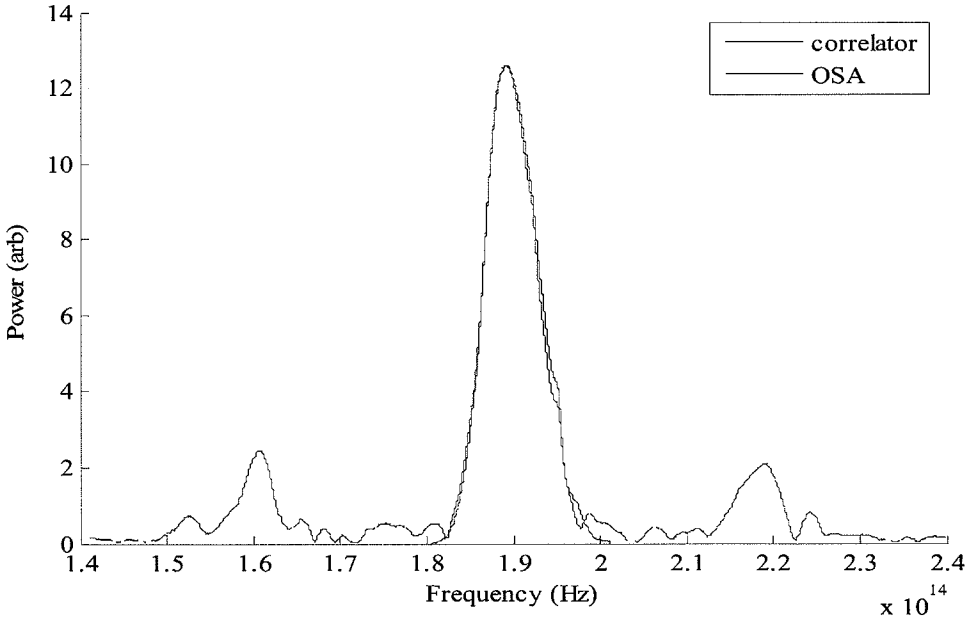

Fig. 4.6: Measured spectrum with stage at 1 mm/s

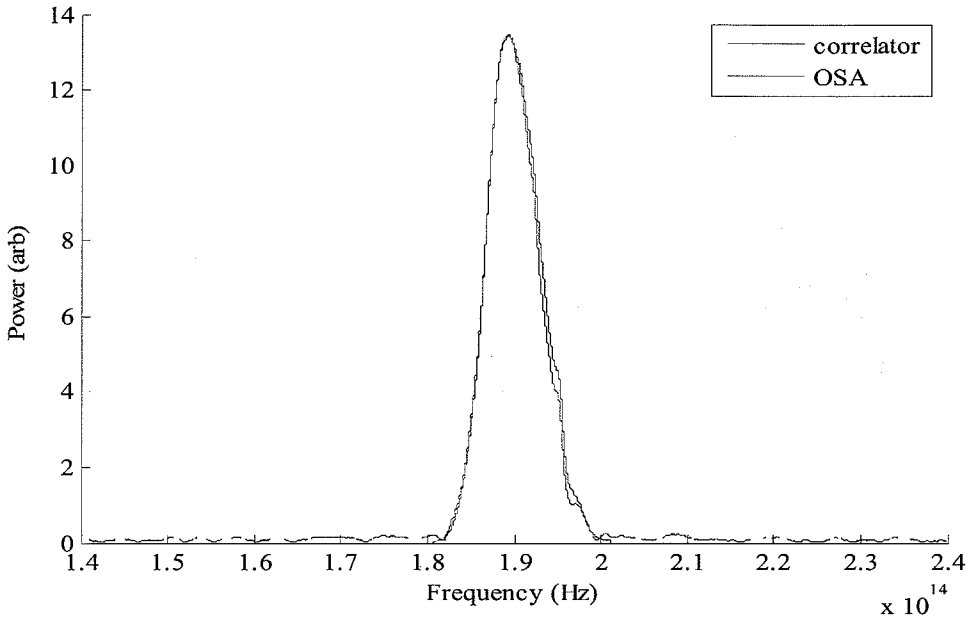

Fig. 4.7: Measured spectrum with stage at .5 mm/s

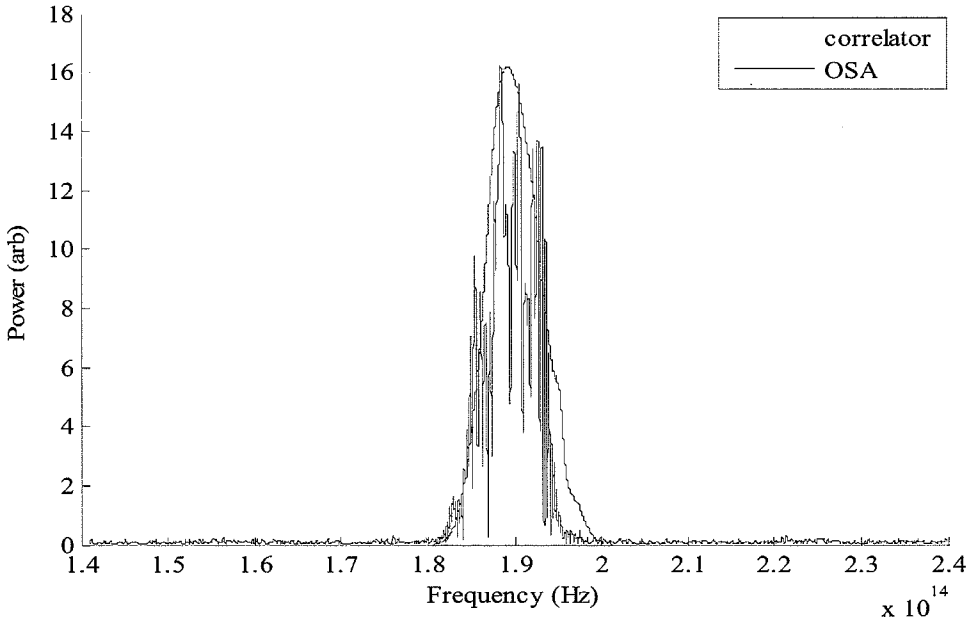

Fig. 4.8: Measured spectrum with stage at .1 mm/s

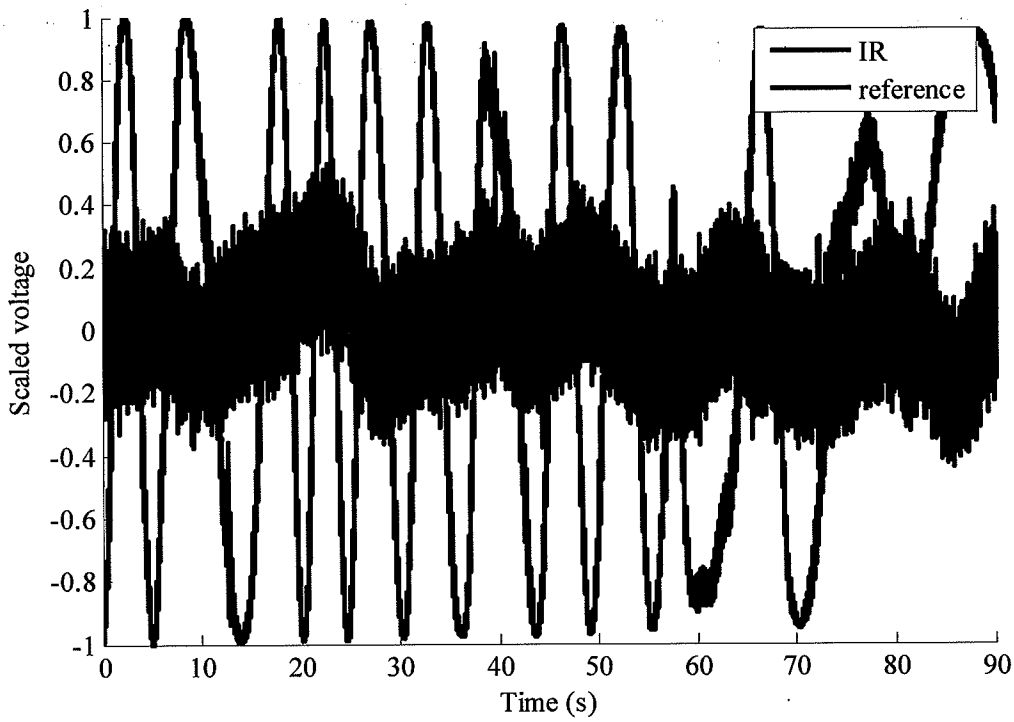

Fig. 4.9: Output of interferometer with zero nominal stage movement

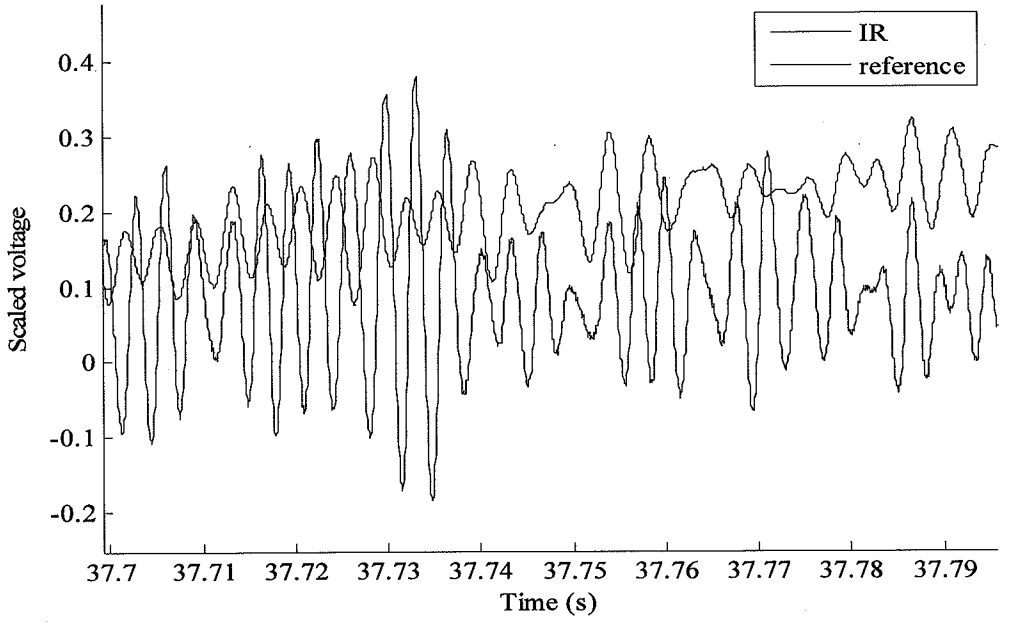

Fig. 4.10: Output of interferometers with zero nominal stage movement

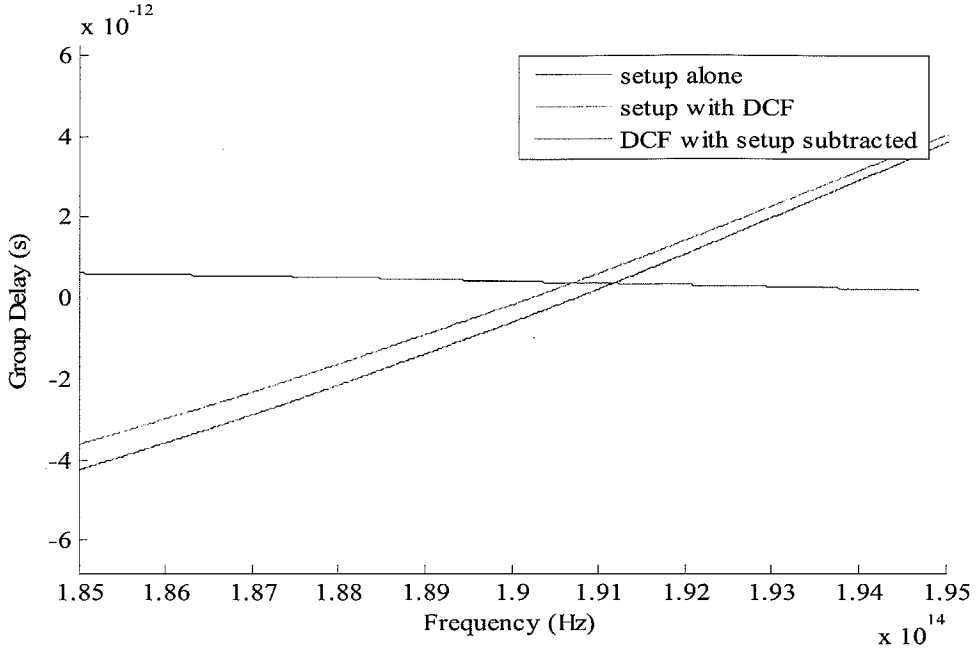

Fig. 4.11: Group delay with setup alone and with DCF

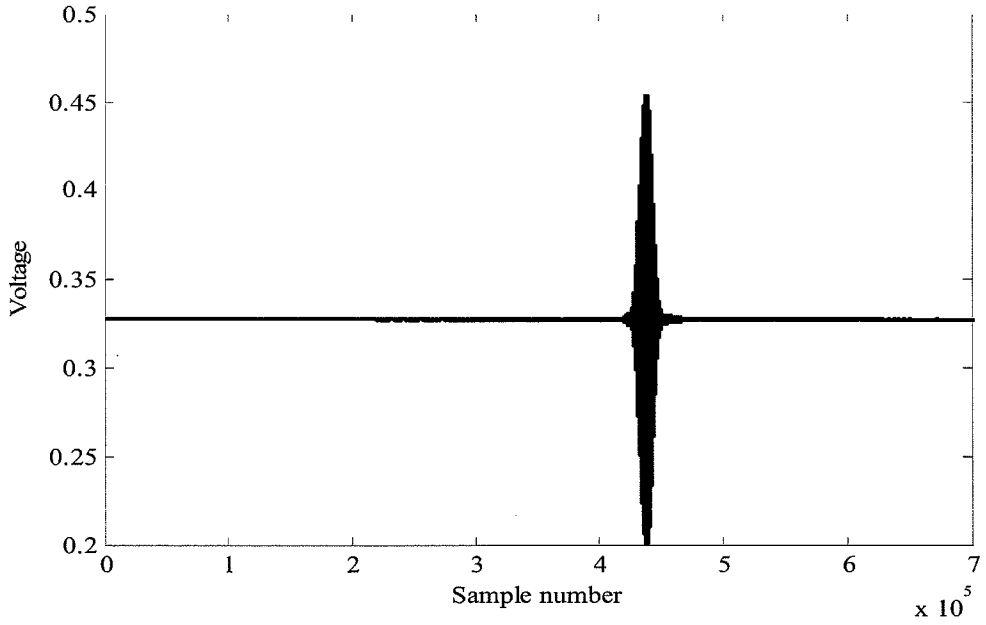

Fig. 4.12: Interferogram of cross correlator alone

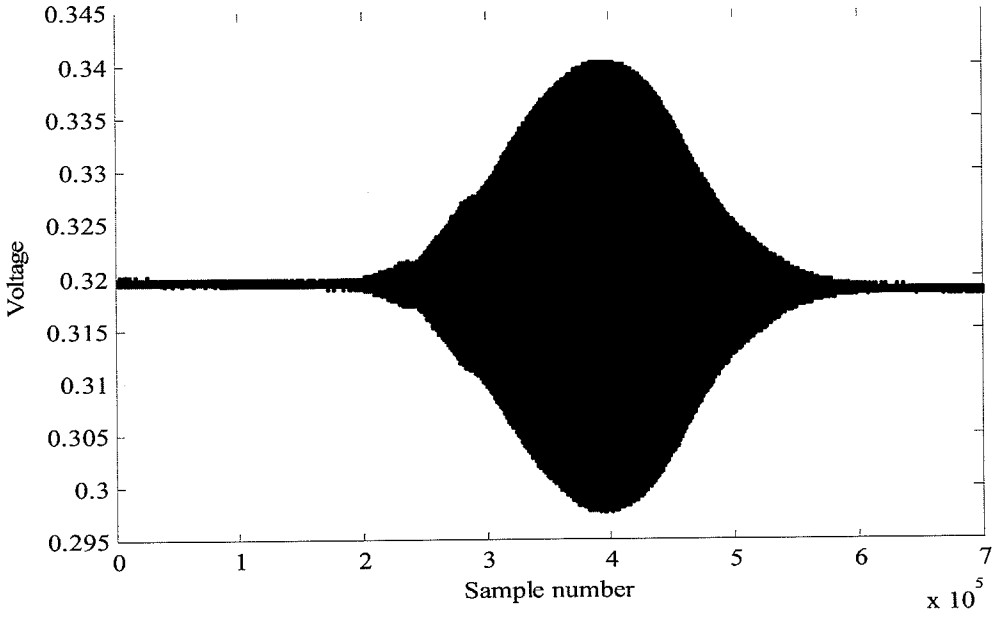

Fig. 4.13: Interferogram of DCF in cross correlator

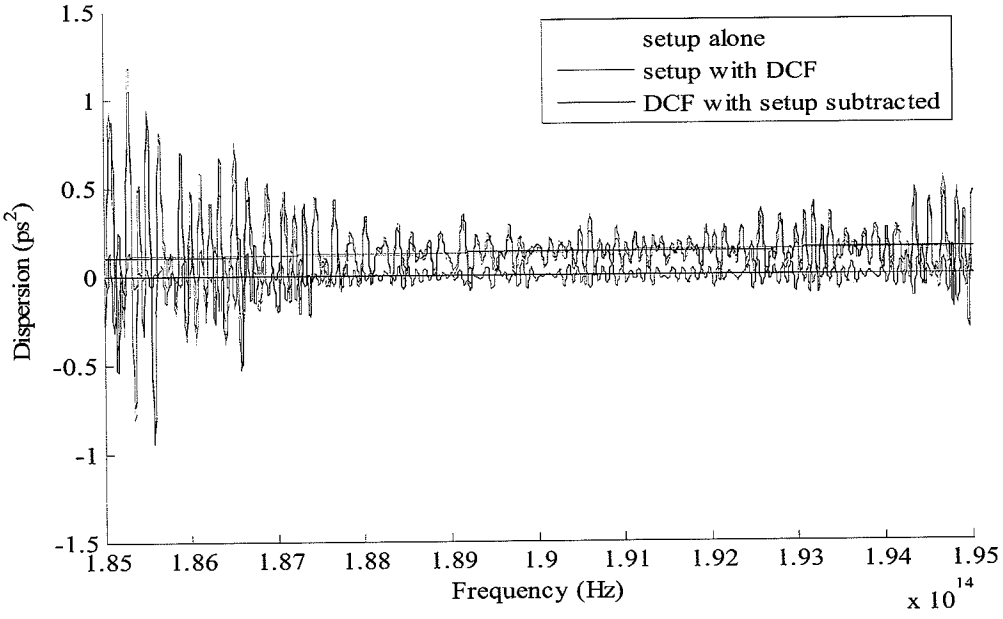

Fig. 4.14: Dispersion of setup alone and with DCF

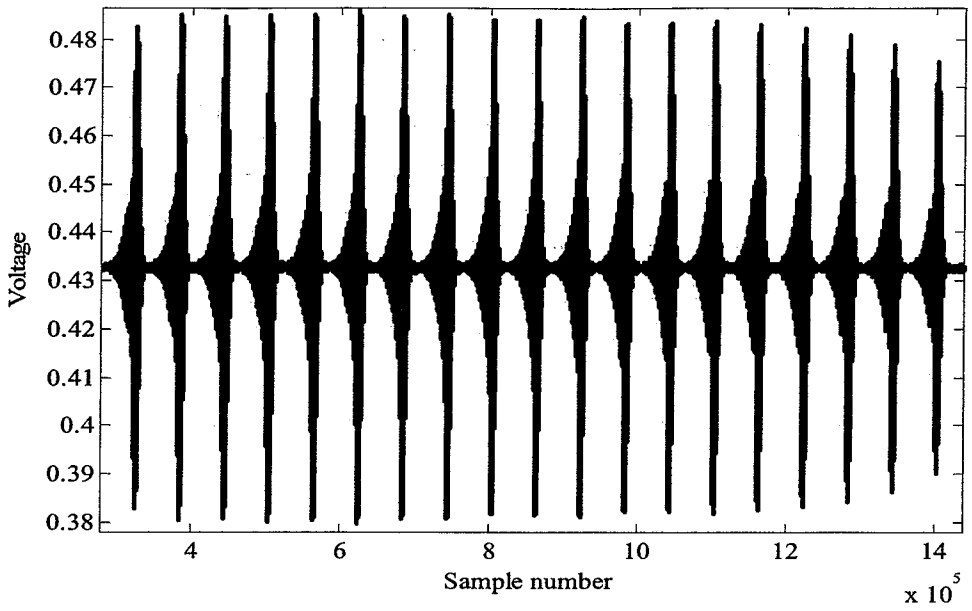

Fig. 4.15: Interferogram of flat topped AWG

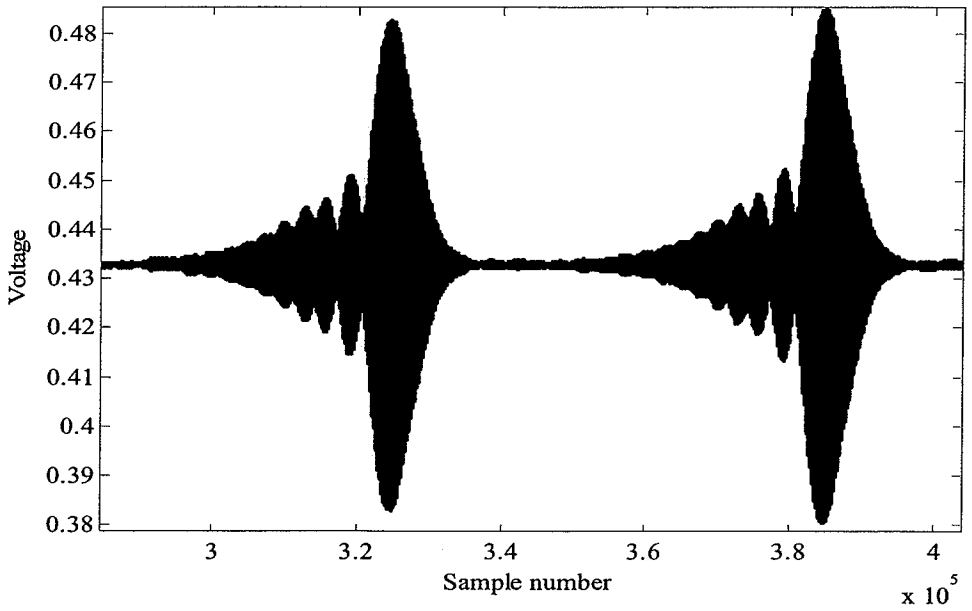

Fig. 4.16: Detail view of Fig. 4.15: Interferogram of flat topped AWG

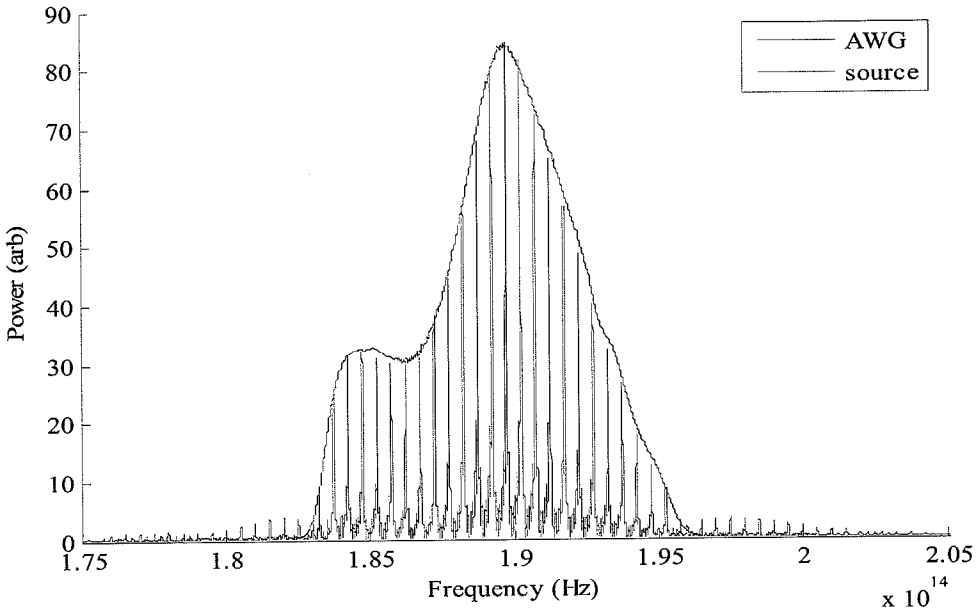

Fig. 4.17: Spectrum of AWG vs. OSA measurement of source

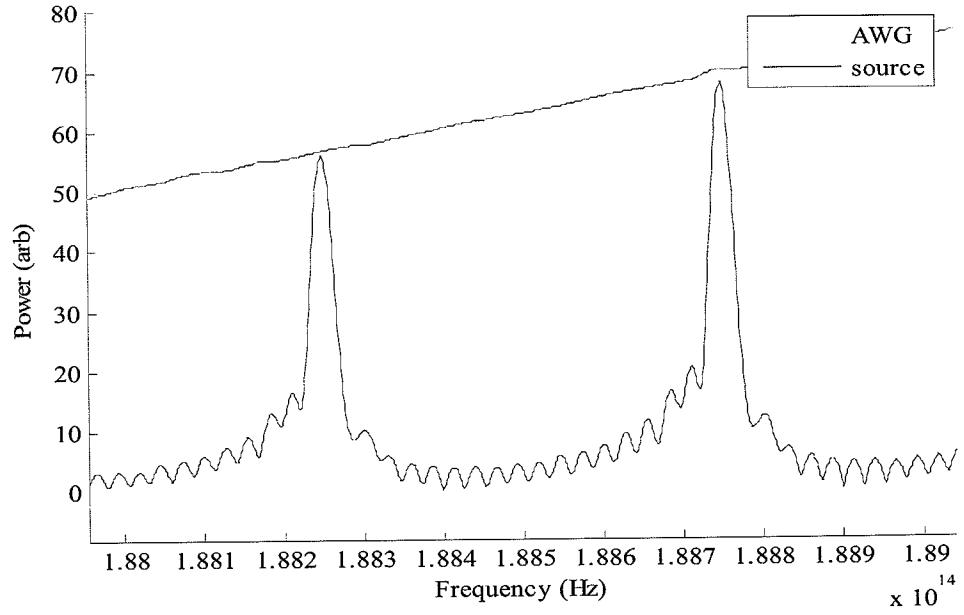

Fig. 4.18: Detail view of Fig. 4.17

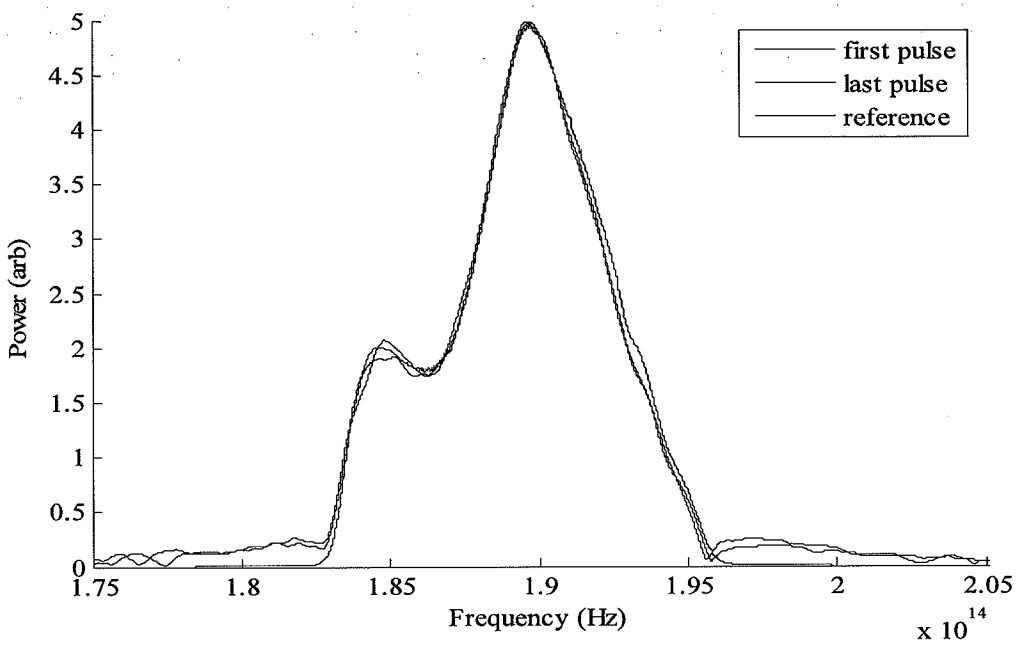

Fig. 4.19: Spectrum of first and last pulse

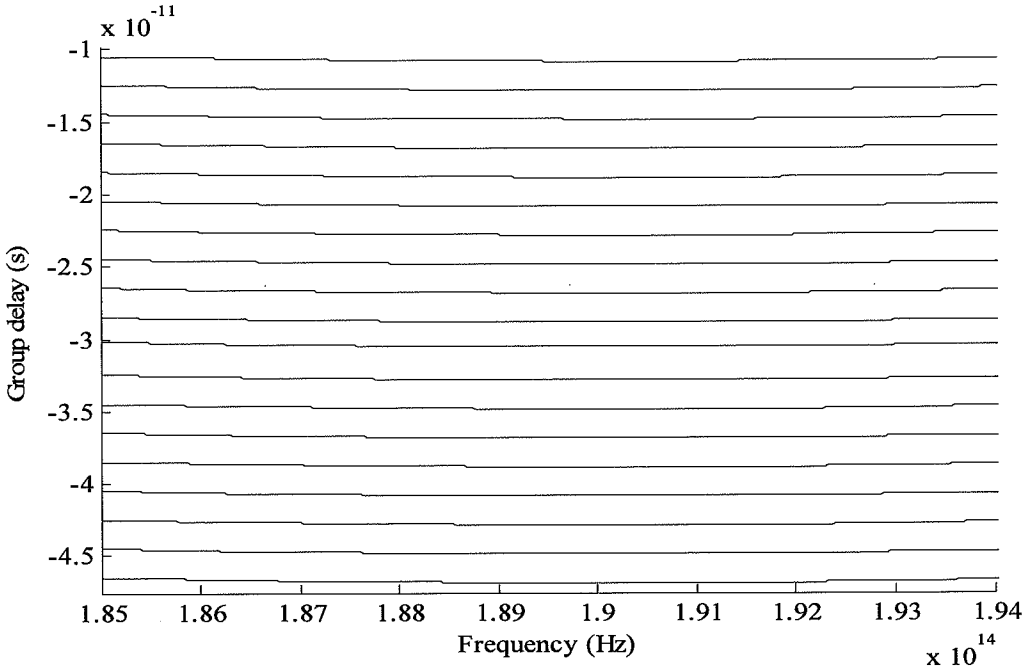

Fig. 4.20: Group delay of pulse through each guide

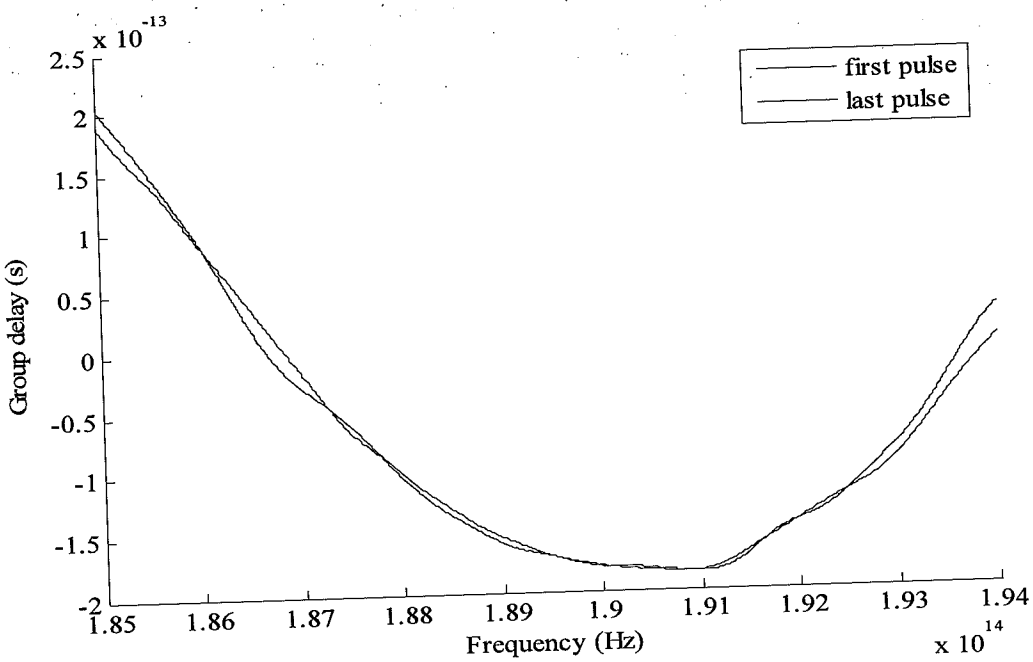

Fig. 4.21: Comparison of normalized group delay

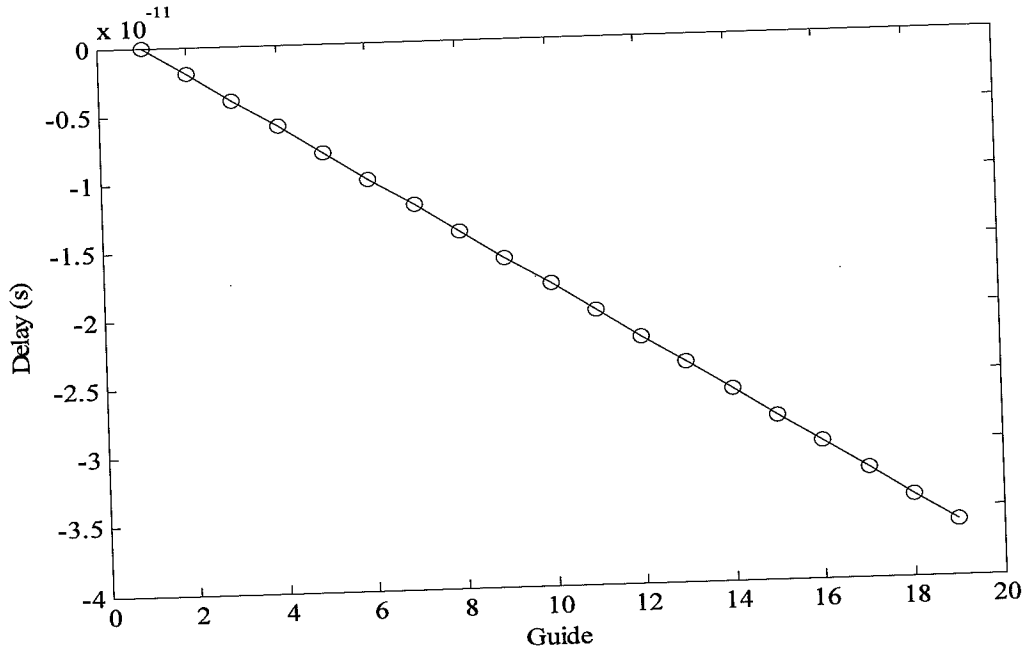

Fig. 4.22: Group delay of peak frequency

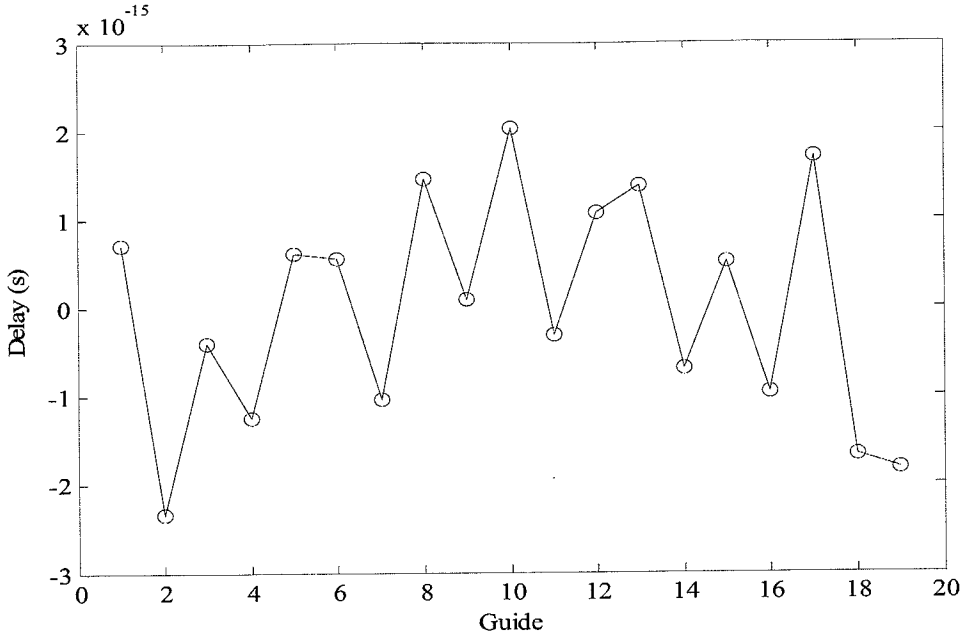

Fig. 4.23: Group delay error

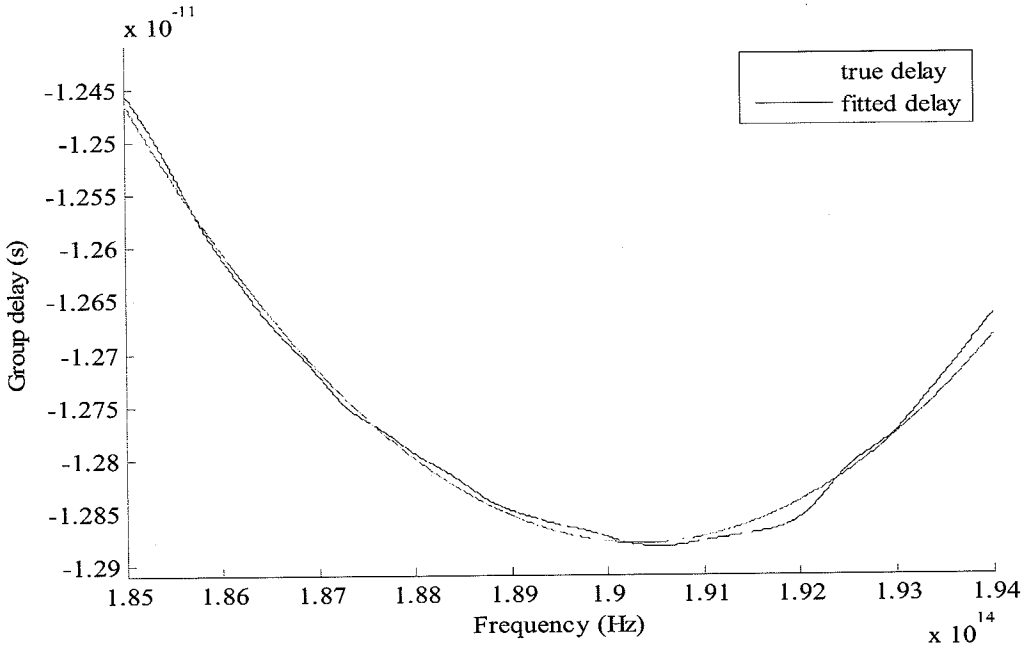

Fig. 4.24: Derivative of fitted phase (3d order polynomial) vs. group delay

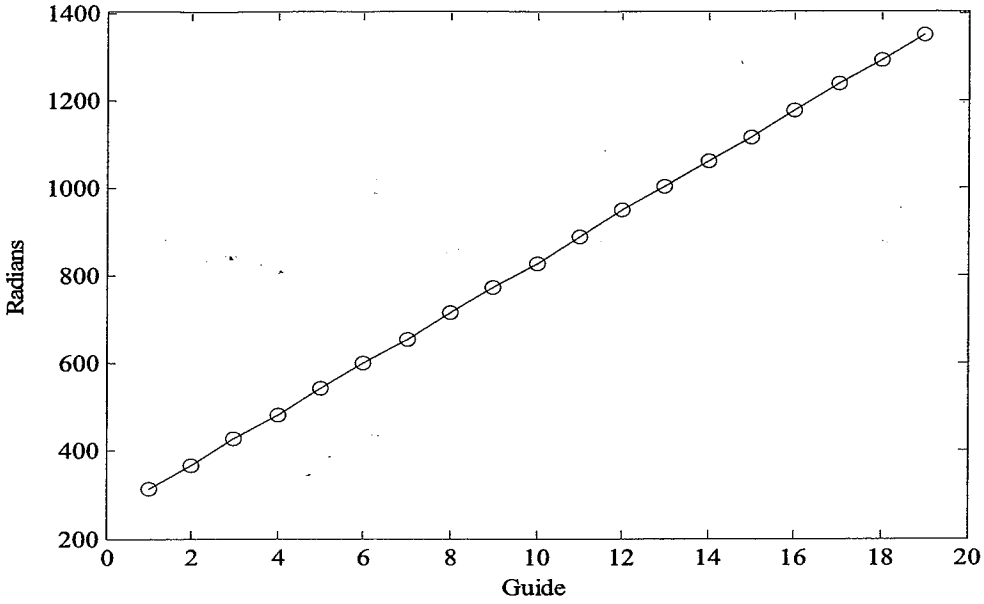

Fig. 4.25: Linear phase of each guide

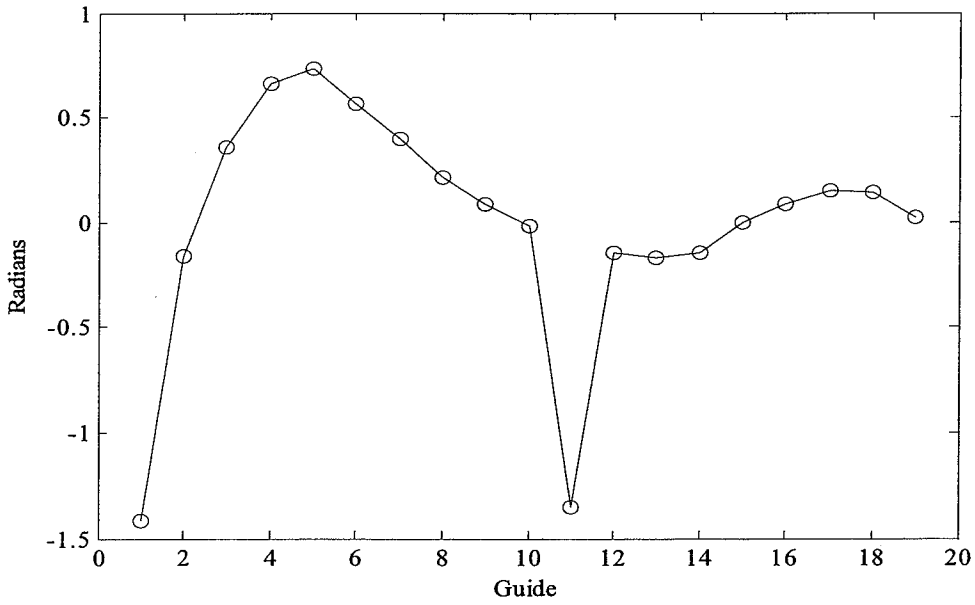

Fig. 4.26: ϕ_0 with linear phase term removed

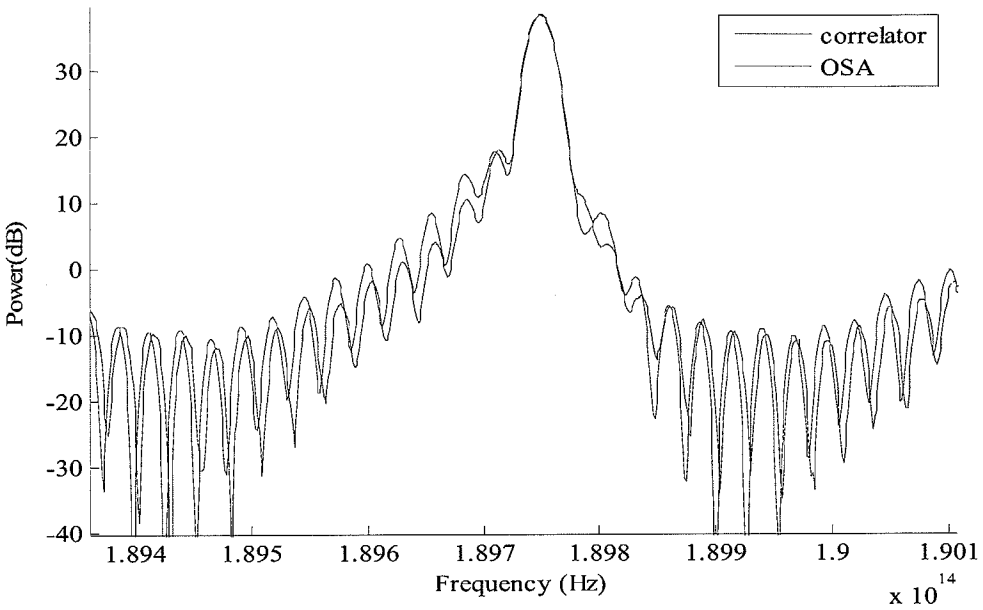

Fig. 4.27: Measured AWG output vs. OSA reference measurement

CHAPTER 5. POLARIMETER

This chapter describes the optimization of a wavelength-parallel polarimeter. The goal was to replace the control of an existing wavelength-parallel polarimeter to permit operation at a rate greater than 1 kHz, which would allow the polarimeter to be used for PMD measurements [11]. To fully characterize the state of polarization, 4 independent measurements are needed since there are four degrees of freedom: two independent linear polarizations, circular polarization, and power. The original setup consisted of an NI 6111 DAQ, a PC, two FLCs, a polarizer, and a camera [11]. The FLCs act as switchable quarter-wave plates, so two FLCs are sufficient to measure four independent polarizations. The layout is shown in Fig. 5.1. In the original design, the computer would set the FLCs to a particular state, trigger the camera to capture a frame, set the DAQ to acquire data, and wait for data to be successfully acquired four times for each complete state of polarization measurement. Each of the software operations was done through one or more system calls, which the operating system would service after an arbitrary period of time on the order of 1 ms. The total time to take one set of data was 23ms +/- 5ms. In order to bring the acquisition time below 1 ms, all software operations were taken out of the critical loop. An external circuit using discrete ICs was built to set the FLCs and trigger the camera to take data and the DAQ was set to automatically respond and capture data upon being triggered by the camera. The circuit consists of two D flip flops, and two inverters, and a variable capacitor. The main input is a square wave generated by the DAQ board, which goes into the clock of the first flip flop. A 2x clock divider is created from each flip flop by wiring the input signal to the flip flop clock, and the flip flop input to the inverted output of the flip flop, and then taking the output of the flip flop as the output. The two flip flops are cascaded to give a ½ speed clock as well as a ¼ speed clock. Additionally, the input is also connected to an inverter which is connected to

another inverter with a variable capacitor in between so a delayed copy of the input clock with an adjustable delay is available. The ½ and ¼ speed clocks are used to switch the FLCs into four independent states by connecting each clock to an FLC and the delayed clock is used to trigger the camera to take data. The delay is needed because the FLCs have non-zero switching time. In the new version, the only thing the software is responsible for is periodically offloading the data from the DAQ, and then saving the data to disk. Since this process is double buffered – data from one DAQ buffer is saved to disk while the DAQ saves data into another one of its buffers – the software no longer limits the speed of operation. Since the DAQ is fast enough to continuously take data from the camera and the camera has to wait for the FLC to change its state the limiting factor is the switching time of the FLC plus the time it takes for the camera to capture one frame. Graphs of the timing dependencies in both control schemes are shown in Fig. 5.2 and Fig. 5.3. An arrow from one device to another indicates that the device pointed to must wait for the device the arrow originates from before beginning its operation.

Speed testing was done by using a broadband source with some arbitrary fixed polarization. The four polarization measurements taken are of 0, 45, and 90 degree linear polarizations, as well as right hand circular polarization. As the speed of the measurement was increased, the measurement was consistent up to 1.25 kHz. At higher speeds, the FLCs couldn't switch in time, and the measurements were not consistent with the measurements done at lower speeds. Fig. 5.4 shows some of the measurements taken at different speeds.

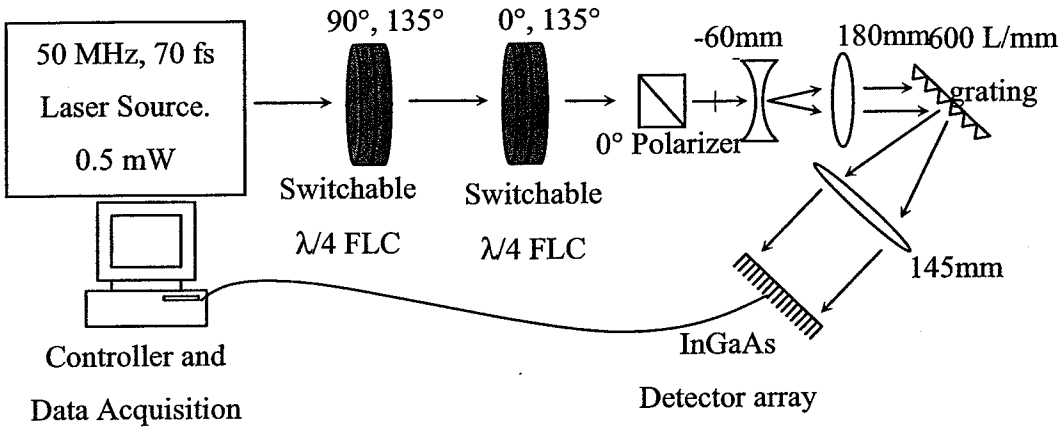

Fig. 5.1: Polarimeter setup

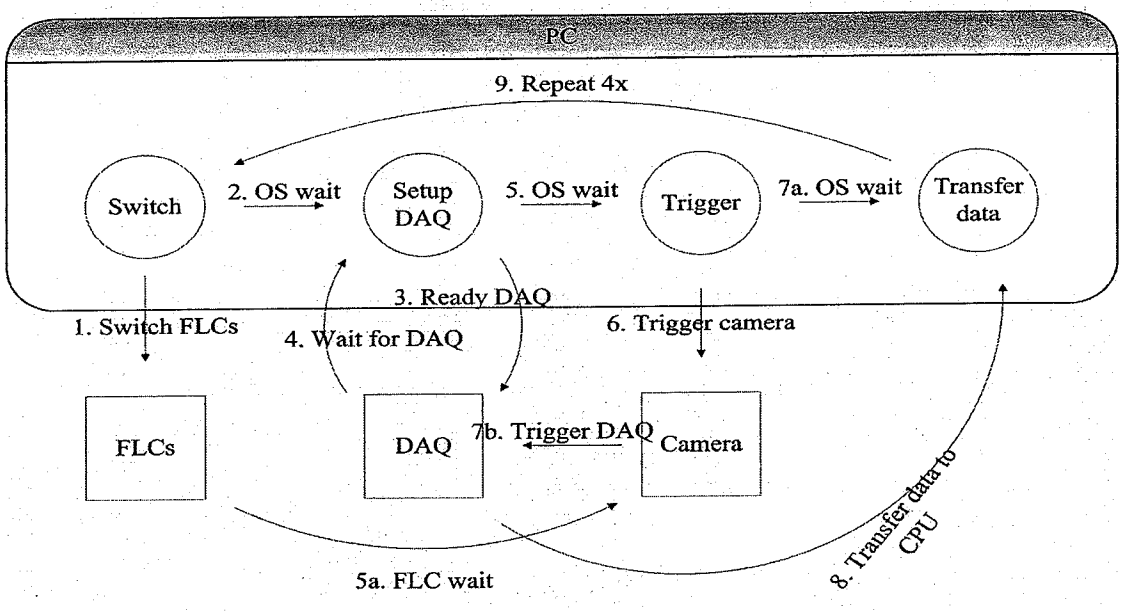

Fig. 5.2: Dependency graph of original setup

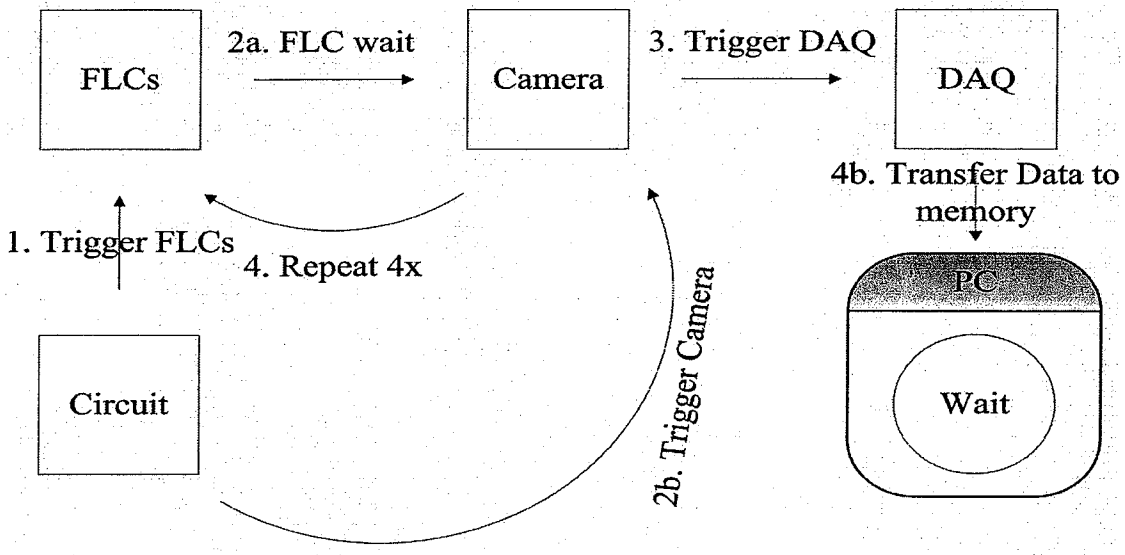

Fig. 5.3: Dependency graph of modified setup

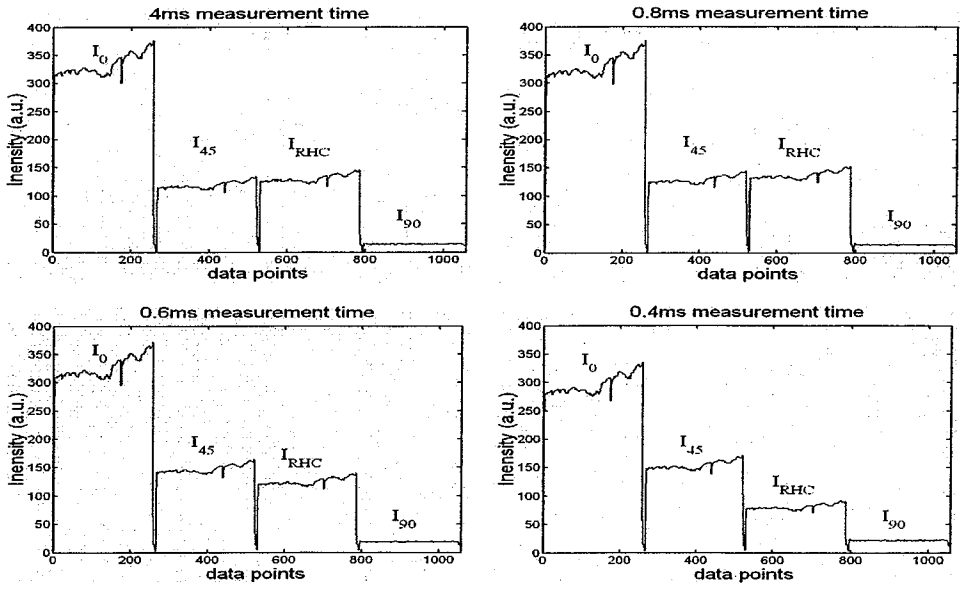

Fig. 5.4: Polarimeter measurement at different speeds [11]

LIST OF REFERENCES

LIST OF REFERENCES

[1] A.M. Weiner, Ultrafast Optics. Unpublished notes, 2004.

[2] P.-L. Francois, M. Monerie, C. Vassallo, Y. Durtese, and F. R. Alard, "Three Ways to Implement Interferencial Techniques: Application to Measurements of Chromatic Dispersion, Birefringence, and Nonlinear Susceptibilities," *Journal of Lightwave Technology*, vol. 1, pp. 500-514, 1989.

[3] R. Trebino, K. W. DeLong, D. N. Fittinghoff, J. N. Sweetser, M. A. Krumbugel, and B. A. Richman, "Measuring ultrashort laser pulses in the time-frequency domain using frequency-resolved optical gating," *Rev. Sci. Instrum.*, vol. 68, pp. 3277–3295, 1997.

[4] C. Iaconis and I. A. Walmsley, "Self-referencing spectral interferometry for measuring ultrashort optical pulses," *IEEE Journal of Quantum Electronics*, vol. 35, pp. 501–509, 1999.

[5] J.H Chung, and A.M. Weiner, "Ambiguity of ultrashort pulse shapes retrieved from the intensity autocorrelation and the power spectrum," *IEEE Journal on Selected Topics in Quantum Electronics*, vol. 7, pp. 656-666, 2001.

[6] M. A. McHenry and D.C. Chang, "Interferometric Method for Chromatic Dispersion Measurement in a Single-Mode Optical Fiber," *IEEE Journal of Quantum Electronics*, vol. 17, pp. 404-407, 1981.

[7] D.E. Leaird, A.M. Weiner, S. Shen, A. Sugata, S. Kamei, M. Ishi, and K. Okamoto, "High repetition rate femtosecond WDM pulse generation using direct space-to-time pulse shapers and arrayed waveguide gratings," *Optical and Quantum Electronics*, vol. 33, pp. 811-826, 2001.

[8] G. Brinkman, N. Abel, "Photonics research experiment: Interferometers for position measurement and spectrum determination". Unpublished report, 2002.

[9] H. Yamada, K. Okamoto, A, Kaneko, and A. Sugita, "Dispersion resulting from phase and amplitude errors in arrayed-waveguide grating multiplexers–demultiplexers," *Optics Letters*, vol. 25, pp. 569-572, 2000.

[10] M.G. Thompson, D. Brady, S.W. Roberts, "Chromatic dispersion and bandshape improvement of SOI flatband AWG multi/demultiplexers by phase-error correction," *IEEE Photonics Technology Letters*, vol. 15, pp. 924-926, 2003.

[11] S.X. Wang, and A.M. Weiner, "Fast wavelength-parallel polarimeter for broadband optical networks," *Optics Letters*, vol. 29, pp. 923-925, 2004.

[12] J. Kauppinen, J. Partanen, *Fourier Transforms in Spectroscopy*. Wiley-VCH, 2001.

[13] S.G. Lipson, H Lipson, and D.S. Tannhauser, *Optical Physics*. Cambridge University Press, 1995.

[14] S. Lidgate, *Advanced Finite Difference – Beam Propagation Method Analysis of Complex Components*, Ph.D. Thesis, George Green Institute for Electromagnetics Research, University of Nottingham, 2004.

[15] D. E. Leaird, Member, A. M. Weiner, S. Kamei, M. Ishii, A. Sugita, and K. Okamoto, "Generation of Flat-Topped 500-GHz Pulse Bursts Using Loss Engineered Arrayed Waveguide Gratings," *IEEE Photonics Technology Letters*, vol. 14, pp. 816-818, 2002.

[16] V. Laude, "Noise analysis of the measurement of group delay in Fourier white-light interferometric cross correlation," *Journal of the Optical Society of America*, vol. 19, pp. 1001-1008, 2002.

[17] N.R. Lomb, "Least-squares frequency analysis of unequally spaced data," *Astrophysics and Space Science*, vol. 39, pp. 447-462, 1976.

[18] J.D. Scargle, "Studies in astronomical time series analysis. II. Statistical aspects of spectral analysis of unevenly spaced data," *Astrophysics Journal*, vol. 263, pp. 835-853, 1982.

[19] A. Savitzky and M. J. E. Golay, "Smoothing and Differentiation of Data by Simplified Least Squares Procedures," *Analytical Chemistry*, vol. 36, pp. 1627-1639, 1964.

[20] P. A. Gorry, "General Least-Squares Smoothing and Differentiation by the Convolution (Savitzky-Golay) Method," *Analytical Chemistry*, vol. 62, pp. 570-573, 1990.

[21] W. Chen, Y.-J. Chen, M. Yang, B. McGinnis, Z. Wu, "Improved techniques for the measurement of phase error in waveguide based optical devices," *Journal of Lightwave Technology*, vol. 21, pp. 198-205, 2003